

Phase Separation Dynamics of Metallic Glass Using Cahn-Hilliard Equation: A Computational Study

Project Report submitted to the Central University of Punjab
For the Award of
Master of Science
In
Physics (Computational Physics)

By
Kabir Thakur
Supervisor
Dr. Dharmendra Singh



Department of Computational Sciences
School of Basic Sciences
Central University of Punjab, Bathinda
2022

DECLARATION

I declare that the work presented in this dissertation called ‘Phase separation dynamics of metallic glass using Cahn-Hilliard equation: A Computational Study’ is my own. This work has been carried out under the guidance of Dr. Dharmendra Singh, Assistant Professor, Department of Computational Sciences at Central University of Punjab. No part of this dissertation has been for the award of any other degree of any other university.

Kabir Thakur
Department of Computational Sciences
School of Basic Sciences
Central University of Punjab, Bathinda - 151401

CERTIFICATE

I certify that Kabir Thakur has prepared his dissertation entitled ‘Phase separation dynamics of metallic glass using Cahn-Hilliard equation: A Computational Study’ , for the award of M.Sc. Physics (Computational Physics) degree at the Central University Punjab, under my guidance. He has carried out this work at the Department of Computational Sciences, School of Basic Sciences, Central University of Punjab.

Dr. Dharmendra Singh
Assistant Professor
Department of Computational Sciences
School of Basic Sciences
Central University of Punjab, Bathinda - 151401

Acknowledgement

I would like to thank Dr. Dharmendra Singh for guiding me through my project work. I would also like to thank all the faculty of Department of Computational Sciences for their help and support. Additionally I would like to thank Dr. Krishnakanta Mondal for helping me understand various mathematical concepts. My heartfelt gratitude to my parents for their constant support and encouragement. I would also like to thank my classmates who have helped me throughout my study.

Kabir Thakur

Abstract

Two numerical techniques namely Finite Difference Method and Spectral Method, have been used along with the Euler Explicit method to study phase transformations in metallic alloys by solving the Cahn-Hilliard equation. Theoretical basis for thermodynamic models is discussed along with the need for a modified Fick's second law of diffusion to account for energy relating to interfaces. The two methods are programmed in MATLAB and optimised for time-step dt and total time-steps. The Spectral Method is shown to be more accurate, stable and efficient as compared to the Finite Difference Method. Both methods are also used simulate microstructures arising due to phase separation caused by various initial composition profiles.

Contents

1	Introduction	8
1.1	Solution Models	9
1.1.1	Ideal Solution Model	12
1.1.2	Regular Solution Model	12
1.1.3	Ordered Solution Model	13
1.2	Phase Diagrams	13
1.3	Chemical Potential	18
1.4	Fickian Diffusion	19
1.4.1	Diffusion and Chemical Potential	19
1.4.2	Fick's Laws	21
1.4.3	Failure of Diffusion Equation	23
1.5	Cahn-Hilliard Equation	24
2	Methodology	28
2.1	Simulation Parameters	28
2.1.1	Boundary Conditions	29
2.2	Numerical Methods	30
2.2.1	Euler Explicit Method	30
2.2.2	Finite Difference Method	30
2.2.3	Spectral Method	31
3	Results and Analysis	33
3.1	Finite Difference Approach	33
3.2	Spectral Method	36
4	Conclusion and Future Scope of Work	40
	Appendix A - Finite Difference method	41
	Appendix B - Spectral Method	43
	References	45

List of Figures

1	Atom types A and B of a binary alloy $A_{1-x}B_x$	10
2	Free energy as a consequence of entropy and enthalpy	13
3	Free energy vs composition for a phase separated system	14
4	Free Energy vs composition for temperatures decreasing from bottom to top plotted in MATLAB	15
5	Phase Diagram for Binary Alloy showing miscibility dome and spinodal region plotted in MATLAB	15
6	From free energy vs composition curve to phase diagram.	16
7	Molar free energy vs composition with chemical potential using tangent line	19
8	Free energy vs composition with chemical potential for $\Omega < 0$	20
9	Free energy vs composition with chemical potential for $\Omega > 0$	21
10	Diffusion and Phase Separation of two systems at different compositions	21
11	Evolution of 1D sinusoidal composition profile with time. Blue line corresponds to $t = 0$ and red line corresponds to $t > 0$	23
12	System configurations based on solution models	24
13	Periodic Boundary Condition	29
14	Total time step optimisation for $dt = 0.001$ $\kappa = 0.5$ $c = 0.3$ using the finite difference method.	33
15	Total time step optimisation for $dt = 0.01$ $\kappa = 0.5$ $c = 0.3$ using the finite difference method.	34
16	Phase separated systems with varying initial composition simulated using finite difference method for $dt = 0.01$ $\kappa = 0.5$ $total - time - steps = 12000$	35
17	Time-step(dt) optimisation with $\kappa = 0.5$ $total - time - steps = 80$ for spectral method solution	37
18	Spectral Method simulationn of $c_0 = 0.7$ which did not converge for $dt = 1.0$ $\kappa = 0.5$ $total - time - steps = 80$	37
19	Phase separated systems with varying initial composition simulated using spectral method for $dt = 1.0$ $\kappa = 0.5$ $total - time - steps = 120$	38

List of Abbreviations

BMG Bulk Metallic Glasses

CH Cahn-Hilliard

FFT Fast Fourier Transform

GFE Gibbs Free Energy

NaN Not a Number

PBC Periodic Boundary Conditions

RVE Representation Volume Element

1 Introduction

When two metals are mixed at a very high temperature, the arrangement of atoms is completely random. When this molten alloy is quenched, the metal does not get enough time to form an ordered structure. Thus an amorphous metal is created. The amorphous nature of this metal gives it glass-like properties. Hence the name Metallic Glasses, also called Bulk Metallic Glasses.

Metallic glass is an emerging class of materials. They can have several interesting properties depending on the microstructures that form during the cooling period of an alloy system[1]. Recently studies into the glass-forming ability of alloys have led to the synthesis of several Bulk Metallic Glasses (BMG) s, which can now be made up to several millimetres thick[5]. This has generated significant interest in BMG s since now their properties can be easily investigated.

The main goal of this thesis is to study the equation that dictates the dynamics of the phase change in these metallic glasses. The Cahn-Hilliard equation [6] derived by Cahn and Hilliard in 1958 is the basis for our study. We consider the alloy system as a phase-field of compositions and study the changes in phase with time. Through Phase-Field Modelling, we are able to study the microstructures that arise in metallic glass systems as a consequence of phase separation. One particular area of interest is the conditions under which the system spontaneously phase separates without having to cross a nucleation barrier and form droplet-like microstructures. This is called spinodal decomposition. Evidence of spinodal decomposition was first reported in the 1940s by Bradley [3] as sidebands in the Bragg peaks of Cu-Ni-Fe alloy. The separation of phase was initially thought of as an uphill diffusion or a negative diffusion coefficient. However, when used with Fick's law of diffusion, the results were incorrect [6]. Part of the literature review for this thesis is devoted to studying how Fick's Law and subsequently the diffusion equation fails to predict the flow of the phase-field for the binary alloy system.

The thermodynamic basis for our study of the binary alloy system is the Gibbs Free Energy (GFE).

$$\Delta G^{mix} = \Omega(1 - \chi_B)\chi_B + RT[(1 - \chi_B)\ln(1 - \chi_B) + \chi_B\ln\chi_B]$$

The system always tries to minimise GFE to attain an equilibrium state. The failure of the diffusion equation to predict the phase-field dynamics revealed to Cahn and Hilliard that the conventional expression for GFE derived by considering a binary alloy system with only configurational entropy is necessary but not sufficient to explain the phase flow.

What we miss out in this expression is the ‘interfacial energy’ which is attributed to the interfaces between two separated phases. To account for the interfacial energy, Cahn

treated the GFE as a functional dependent on the composition as well as its derivatives.

$$G = \int F(x, y, z, c, \nabla c, \nabla^2 c) dV$$

With knowledge of some variational calculus and tensors, one can derive the Cahn Hilliard Equation [6]. This derivation is covered in section 1.5.

$$\frac{\partial c}{\partial t} = D\nabla^2 \left[\frac{\partial f}{\partial c} - 2k\nabla^2 c \right]$$

The main purpose of this study is to investigate the Cahn-Hilliard (CH) equation by simulating it in 2 dimensions using finite difference and spectral schemes. By studying the microstructures formed due to various parameters of the system computationally, we aim to understand what factors drive the system towards phase separation. A study into the phases formed with various initial concentrations is also of significant interest as changing the composition is easiest to achieve experimentally.

The finite difference and spectral schemes are widely used for solving partial differential equations. The CH equation proves particularly complex to solve as it includes a fourth-order derivative, a non linear term along with a time dependence. Several numerical methods such as Euler explicit, Euler Implicit, Crank Nicolson etc. are used to solve the time dependence. Different combinations of numerical techniques have been juxtaposed to look for the most efficient algorithm. We also assume periodic boundary conditions in all simulated systems.

Cahn-Hilliard Equation can also have applications outside the framework of spinodal decomposition. It can be used in any situation where diffusion occurs in the presence of very sharp composition gradients.

1.1 Solution Models

We begin by trying to understand several models for thermodynamics of alloy systems. We know that atoms such Nickel, Copper, Zinc crystallise in face centred cubic structures [9]. If we take two different types of atoms and put them together for example Nickel and Copper and mix them, they form a solid solution. If we consider Nickel and Aluminium [14], they form ordered structures while Aluminium and [10] would phase separates. The solution models are used to understand what happens when we take atoms of different types and put them together. The basis for this model is Gibbs Free Energy (GFE). We can write the GFE as

$$G = H - TS \tag{1}$$

For solids and liquids we can make the approximation that $H \approx U([7])$ where The PV term is neglected. We are assuming the system to be constant at normal atmospheric pressure.

So we can write

$$G = U - TS \quad (2)$$

Let us consider a binary alloy with atom types A and B. For this system we can write the GFE as [13]

$$G = \chi_A G_A + \chi_B G_B \quad (3)$$

Where G_A and G_B represent molar free energies of pure A and pure B in figure 1 atoms.

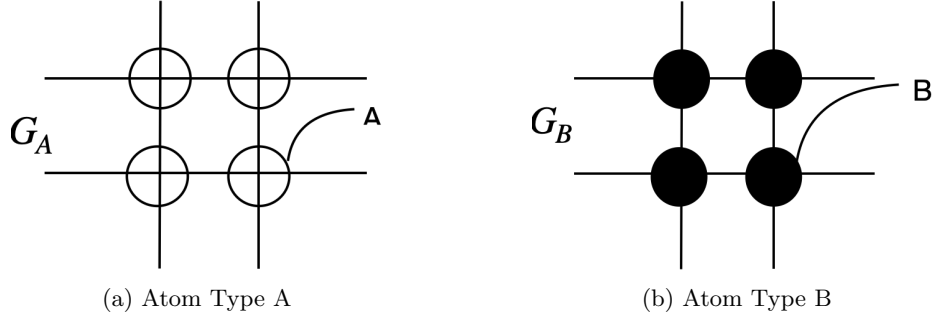


Figure 1: Atom types A and B of a binary alloy $A_{1-x}B_x$

Whenever we distribute these atoms onto a lattice we are generating a configuration. The entropy that is associated with each configuration is known as configurational entropy. The difference between the sum of the stand alone atomic structures and the mixed atomic structures gives us the free energy of mixing as

$$\Delta G^{mix} = \Delta U^{mix} - T\Delta S^{mix} \quad (4)$$

Here we make an assumption that the entropy of the system is only a function of the configuration of the system $\Delta S^{mix} = \Delta S^{mix, configuration}$. From statistical mechanics we know that the configurational entropy can be written as

$$S = k_B \ln \omega \quad (5)$$

where ω is the number of microstates of the system. Suppose we have N_A -A type atoms and N_B -B type atoms and we have to distribute them onto N sites where $N = N_A + N_B$. Here the A type and B type atoms are indistinguishable within themselves and thus the entropy associated with the initial configurations is will be zero. Assuming that there are no defects in our arrangement we can write ω as

$$\omega = \frac{N!}{N_A! N_B!} \quad (6)$$

The difference between the entropy of different configurations can be written as

$$\begin{aligned}\Delta S^{mix, config} &= k \ln \left(\frac{N!}{N_A! N_B!} \right) \\ &= k[\ln N! - \ln N_A! - \ln N_B!]\end{aligned}$$

Using the sterling approximation

$$\ln N! = N \ln N - N \quad (7)$$

We can write

$$\begin{aligned}\Delta S^{mix, config} &= k[N \ln N - N - N_A \ln N_A + N_A - N_B \ln N_B + N_B] \\ &= k[(N_A + N_B) \ln N - N_A \ln N_A - N_B \ln N_B] \\ &= -k \left[N_A \ln \frac{N_A}{N} - N_B \ln \frac{N_B}{N} \right] \\ \therefore \Delta S^{mix, config} &= -k_B N[\chi_A \ln \chi_A + \chi_B \ln \chi_B] \quad (8)\end{aligned}$$

Where χ_A and χ_B are mole fractions

$$\chi_A = \frac{N_A}{N} \quad \text{and} \quad \chi_B = \frac{N_B}{N} \quad \text{and} \quad \chi_A + \chi_B = 1 \quad (9)$$

We can write the internal energy of mixing as [7]

$$\Delta U^{mix} \approx \Delta H^{mix} = \Omega \chi_A \chi_B \quad (10)$$

When

$$\Omega = N_a Z \epsilon \quad (11)$$

Ω is known as the regular solution parameter. N_a is the Avogadro's number, Z is the coordination number for atom and ϵ is given by

$$\epsilon = E_{AB} - \frac{1}{2}[E_{AA} + E_{BB}] \quad (12)$$

So finally we can write the GFE of mixing as

$$\Delta G^{mix} = \Omega \chi_A \chi_B + RT[\chi_A \ln \chi_A + \chi_B \ln \chi_B] \quad (13)$$

1.1.1 Ideal Solution Model

In the case of ideal solution, we assume that the system does not differentiate between A-A, B-B or A-B type bonds.

$$\Omega = 0 \quad (14)$$

$$\Delta U^{mix} = 0 \implies \Delta H^{mix} = 0 \quad (15)$$

And,

$$\therefore N > N_A \implies \ln \frac{N_A}{N} < 0 \quad (16)$$

similarly

$$\therefore N > N_B \implies \ln \frac{N_B}{N} < 0 \quad (17)$$

$$\therefore \Delta G^{mix} < 0$$

We see that the configurational entropy is always going to reduce the free energy. So in a binary alloy system it is always favourable to have mixing as it reduces the overall GFE. In this system the atoms will mix together very well and form a homogeneous solution since the system does not differentiate between AA, BB or AB type bonds. Thus this is called ideal solution. The system itself will choose the arrangement where the GFE is minimised. Ideal solutions do not exist in actuality but the model provides a good reference point for studying other solution models.

1.1.2 Regular Solution Model

In the regular solution model we have

$$\Omega > 0 \quad (18)$$

$$\Delta H^{mix} \neq 0 \quad \text{and} \quad \Delta H^{mix} \ll 1 \quad (19)$$

The full equation for free energy (equation 13) now comes into play unlike in the ideal solution model. At high temperatures the $\Delta S^{mix,config}$ term dominates the GFE while at low temperatures ΔH^{mix} term dominates. This implies that at higher temperatures the arrangement of atoms would be random irrespective of that the value of Ω . While at lower temperatures the enthalpy of mixing will dictate the arrangement of atoms.

Since we have $\Omega > 0$, this implies that $\epsilon > 0$ and therefore

$$E_{AB} > \frac{1}{2}[E_{AA} + E_{BB}] \quad (20)$$

According to this equation AB bonds are costlier than AA and BB bonds. So it is always favourable for the system in this case to phase separate into A rich and B rich regions. The Cahn-Hilliard equation defines the dynamics of the system for the regular solution model

where we observe phase separation in the form of spinodal decomposition

1.1.3 Ordered Solution Model

In the ordered solution model, we have

$$\Omega < 0 \quad (21)$$

Thus,

$$E_{AB} < \frac{1}{2}[E_{AA} + E_{BB}] \quad (22)$$

This means that if there are AA and BB bonds in the system, they will break down to form AB bonds. This phenomenon happens at low temperatures and is known as ordering. The dynamics of an ordered solution are modelled by using the Allen-Cahn equation which is beyond the scope of this project.

1.2 Phase Diagrams

To understand the GFE of alloy systems we write equation 13 in terms of mole fraction χ_B

$$\Delta G^{mix} = \Omega(1 - \chi_B)\chi_B + RT[(1 - \chi_B)\ln(1 - \chi_B) + \chi_B \ln \chi_B] \quad (23)$$

Figure 2 shows the graph for ΔG vs χ_B for $\Omega > 0$

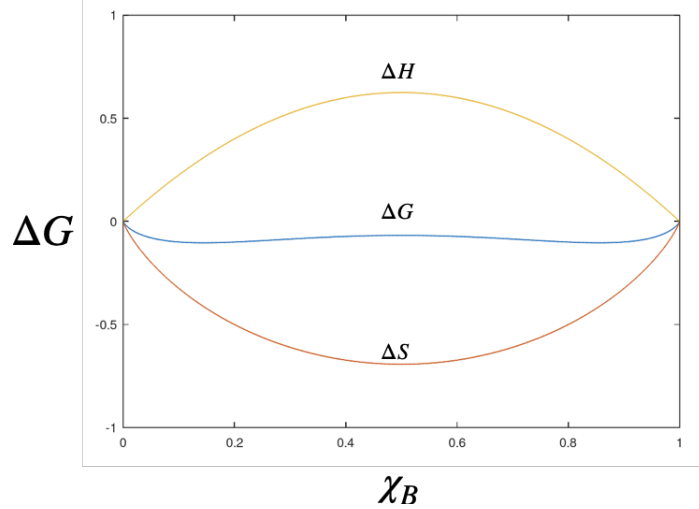


Figure 2: Free energy as a consequence of entropy and enthalpy

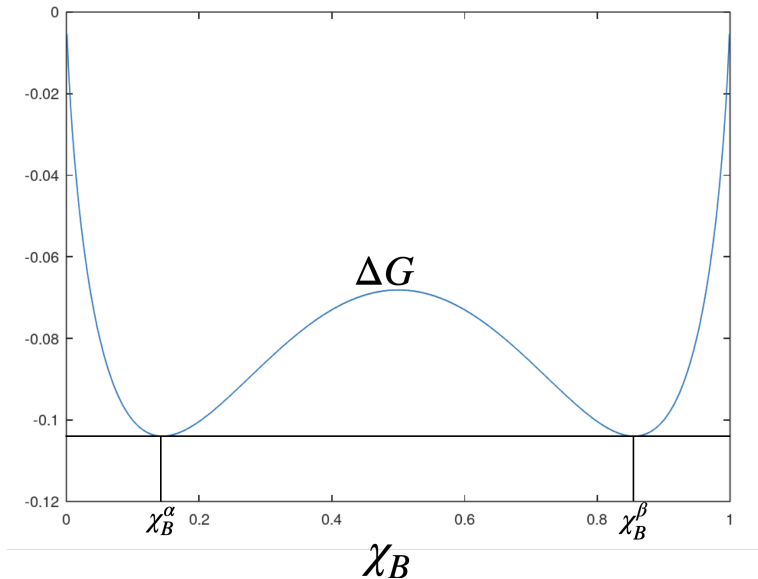


Figure 3: Free energy vs composition for a phase separated system

In figure 2 we observe how the values of ΔS and ΔH effect the values of ΔG . Figure 3 is a magnified plot of ΔG vs χ_B . These figures are commonly referred to as free energy vs composition graphs for a binary system. The left vertical axis of these figures represents a point where mole fraction of A type atoms is high and B is zero while the right vertical axis represents that mole fraction of B type atoms is high and A type atoms is zero. The free energy vs composition curve in figure 3 has been drawn by taking a constant value for temperature. Anytime we see this concavity in our free energy vs composition curve, we observe phase separation. The value of free energy is going to lie somewhere on the tangent connecting the two minima of the curve.

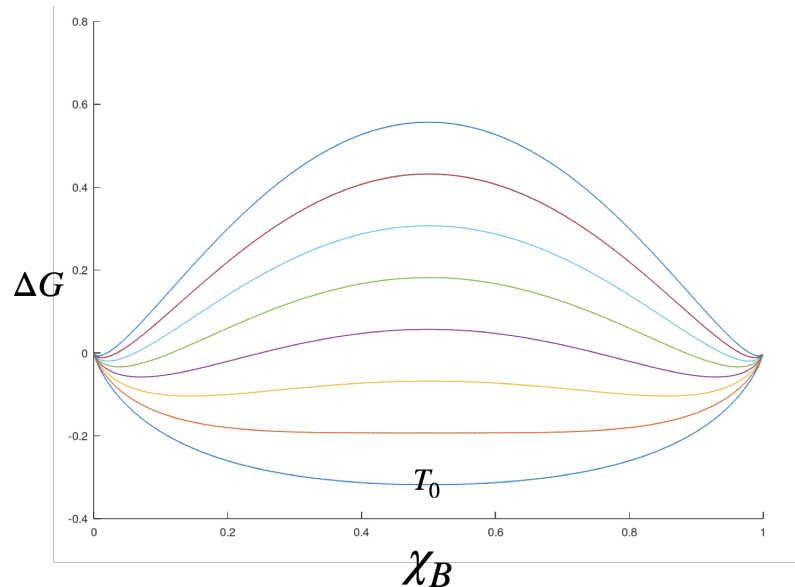


Figure 4: Free Energy vs composition for temperatures decreasing from bottom to top plotted in MATLAB

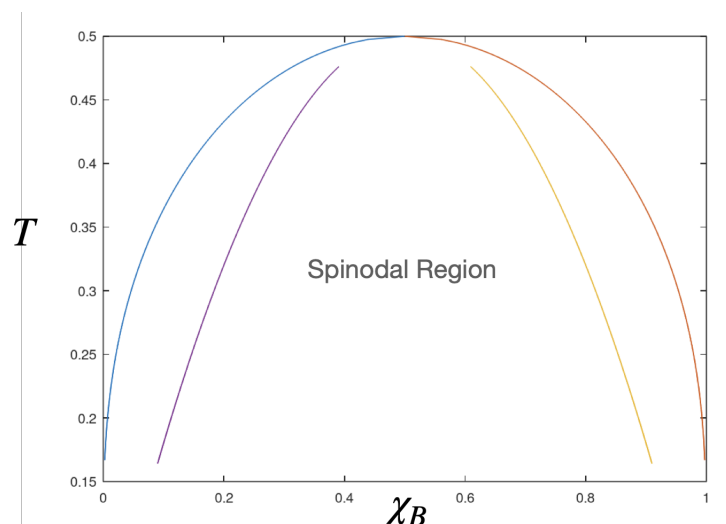


Figure 5: Phase Diagram for Binary Alloy showing miscibility dome and spinodal region plotted in MATLAB

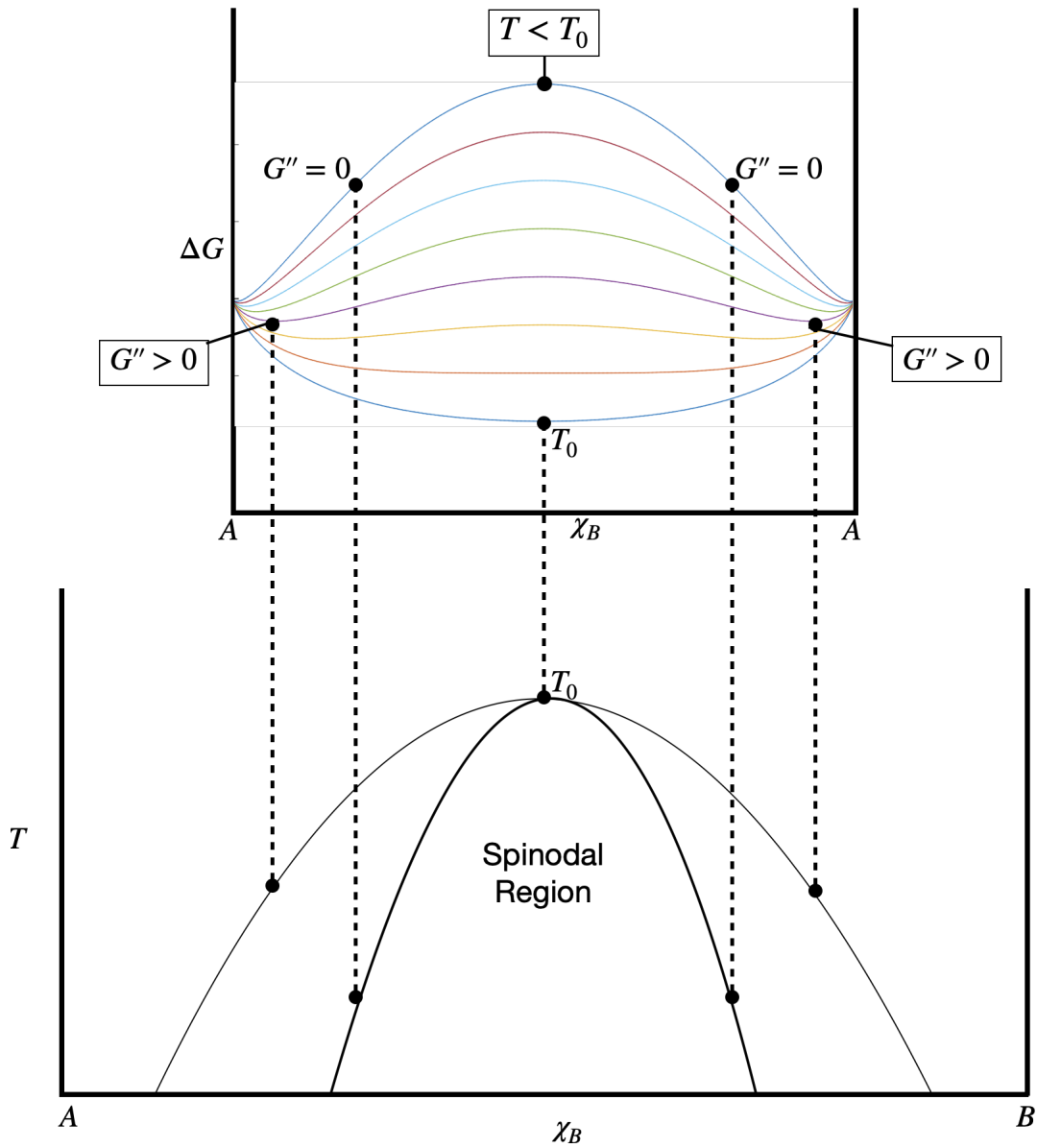


Figure 6: From free energy vs composition curve to phase diagram.

Figure 4 shows the ΔG curves for varying temperature. The curves going from bottom to top correspond to decrease in temperature. At a certain temperature T_0 the values of ΔH starts dominating the middle part the curve while ΔS dominates the edges. Below this critical temperature the system phase separates into a mechanical mixture.

We identify minima of the free energy vs composition curves by drawing a common tangent to the minima on the curve ΔG as shown in figure 3. The point where the tangent meets the curve can be considered as different phases of our composition. This plot for ΔG is for a particular temperature. The phases α and β correspond to two points on the temperature vs χ_B graph. Different temperature values correspond to different ΔG curves as seen in figure 4. Each different plot corresponds to two different points on the temperature vs χ_B graph except for the temperature T_0 where our system is not phase separated. The resulting plot (figure 5) is called a phase diagram and it describes the phases at each temperature. The dome like shape in the graph which is commonly referred to as the miscibility dome or miscibility gap.

The system exists in two phases inside the miscibility gap which means that there is no complete mixing of A type and B type atoms inside this region. At T_0 the system is in only one state and as we decrease the temperature, the system phase separates into A rich and B rich phase.

The curvature of the ΔG curve at the minima can be written as $G'' > 0$ where

$$G'' = \left(\frac{\partial^2 G}{\partial \chi_B^2} \right)_{T,P} \quad (24)$$

and the maxima can be written as $G'' < 0$. In between the maxima and minima there lies a point where $G'' = 0$. Plotting these points which are known as spinodal points for varying temperature values in the phase diagram we get a region inside the miscibility gap known as the spinodal region where $\frac{\partial^2 G}{\partial x^2} = 0$. This kind of phase diagram for ΔG curves where $\Omega > 0$ imply a positive deviation from ideal solution model where $\Omega = 0$. The spinodal region indicates a separation between metastable and unstable states of the system.

At any point inside the spinodal region the system is unstable. At other points inside the miscibility gap but outside the spinodal region the system is metastable. In terms of the free energy curve the metastable state represents a local minima, the maxima represents the barrier that the system needs to cross to get to the global minima of the free energy curve which is the stable state. The points where the second derivative of the GFE is 0 represents the points on the graph between the minima and maxima where the system will spontaneously reach minima without having to cross any barrier. In order for the free energy to reach global minima from local minima the system needs to be pushed far enough to reach instability and overcome a barrier.

Similarly anywhere inside the miscibility gap the system wants to phase separate to A

rich and B rich phase. However in the metastable region the system needs to overcome a nucleation barrier. Inside the spinodal region the system does not have to overcome any barrier so it will phase separate spontaneously.

1.3 Chemical Potential

Let us take a system with constant temperature T and pressure P. Assuming that our system has N_A A type atoms and N_B B type atoms we add a very small number of A type atoms to our system dn_A . The change in free energy due to the added atoms [13]

$$dG' \propto dn_A \implies dG' = \mu_A dn_A \quad (25)$$

Here μ_A is the partial molar free energy of A type atoms in the system and is called the Chemical Potential. Thus, chemical potential of A atoms is the change in free energy when we add a small number of A atoms keeping temperature and pressure constant.

$$\mu_A = \left(\frac{\partial G'}{\partial n_A} \right)_{T,P,n_B}$$

The chemical potential in terms of composition can be written as

$$\mu = \frac{1}{N_v} \frac{\partial G}{\partial c} \quad (26)$$

Change in free energy of a binary system can be written as

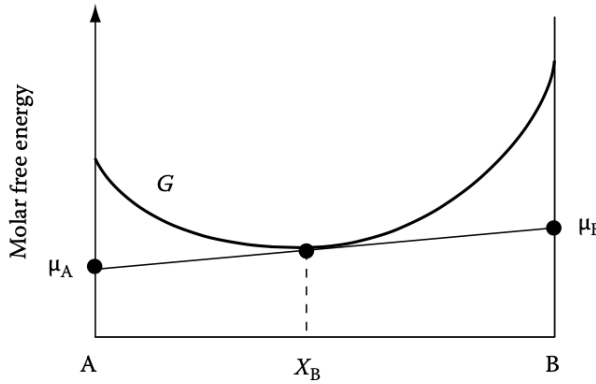
$$dG' = \mu_A dn_A + \mu_B dn_B \quad (27)$$

If we add 1 mol of χ_A and 1 mol of χ_B to the system, the size of the system increases by 1 mol without any change in chemical potential. The GFE in this case will be

$$G = \mu_A \chi_A + \mu_B \chi_B \quad (28)$$

In a free energy vs composition diagram [fig 7], a tangent drawn to the free energy curve gives the value of chemical potential of A wherever the tangent cuts A axis and B wherever the tangent cuts B axis for a given composition χ_B shown by the dashed line.

Chemical Potential helps us understand several properties of the system like atomic flux and the diffusion process. In essence the chemical potential will decide which way the atoms will move. These atoms will be exchanged between the A rich and B rich regions till the chemical potential is equalised.



[13]

Figure 7: Molar free energy vs composition with chemical potential using tangent line

1.4 Fickian Diffusion

Looking at the thermodynamics of the system one can find out if the system will be immiscible, miscible or ordered. So the equilibrium structure formed by our system can mostly be derived by thermodynamics. However we are also concerned about the kinetics of our system to study factors like how long it would take for our system to attain this equilibrium. In all solid-solid systems kinetic processes are dictated by diffusion. If we consider a homogeneous system which is trying to phase separate. The A atoms want to move to one side and B to the other. The time taken by these atoms to move and finally reach equilibrium is determined by their diffusivity. Thus diffusion is an essential process to study while investigating the dynamics of a binary alloy system.

1.4.1 Diffusion and Chemical Potential

We know that the diffusion process will continue in a system till the chemical potentials get equalised and an equilibrium state is attained. Let us consider the following free energy vs composition curves given in figure 8 and 9.

In figure 8 we have chosen two initial compositions χ_1 and χ_2 . The point where the tangent line 1 cuts the A line is the chemical potential μ_1^A similarly where the tangent line 2 cuts the A line is the chemical potential μ_2^A . The chemical potentials μ_1^B and μ_2^B have been defined in a similar fashion. We see that

$$\mu_1^A > \mu_2^A \quad \text{and} \quad \mu_2^B > \mu_1^B \quad (29)$$

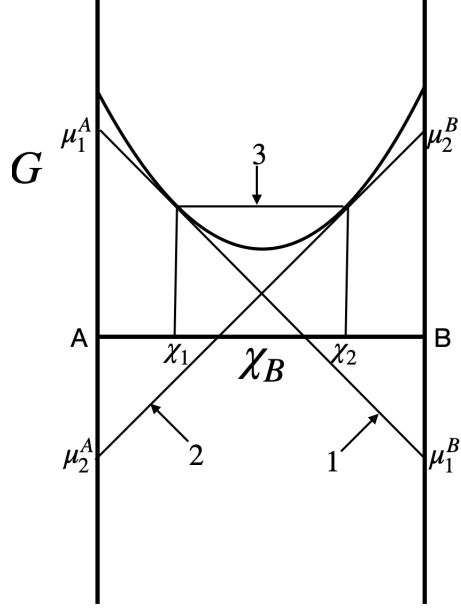


Figure 8: Free energy vs composition with chemical potential for $\Omega < 0$

Now, suppose if we make two systems using initial compositions χ_1 and χ_2 and put them together keeping them at a high enough temperature that the diffusion process can take place. Since the GFE of this system lies somewhere on line 3 in fig 8, we see that in the system 1 (where chemical potential of A is higher than that of system 2) will donate A atoms and since chemical potential of B is lower in system 1 it will receive B atoms. Thus our overall mixture will tend towards homogeneity minimising the GFE as given in figure 10a.

In figure 9 we have a double well system with GFE as in figure 3. Here we see that

$$\mu_1^A < \mu_2^A \quad \text{and} \quad \mu_2^B < \mu_1^B \quad (30)$$

Now if we compare this to the system we had before, A type atoms will flow towards the A rich region and B type atoms will flow towards the B rich region and we will have a mechanical mixture of two phases α and β as given in figure 10b. This behaviour is opposite to that observed for a system with GFE as shown in figure 8. In this case the homogenized system will have a higher GFE than the phase separated system.

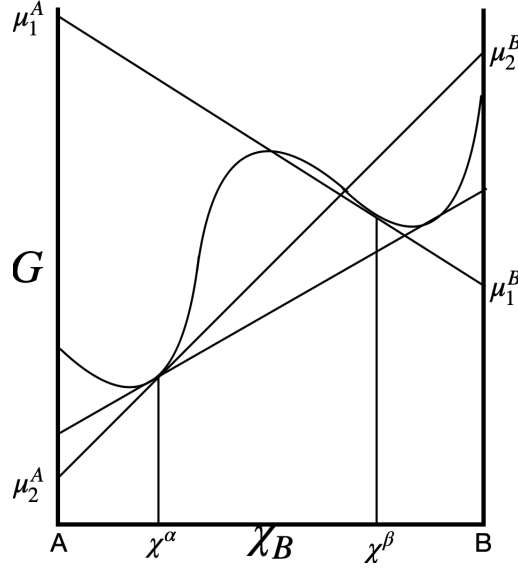


Figure 9: Free energy vs composition with chemical potential for $\Omega > 0$



Figure 10: Diffusion and Phase Separation of two systems at different compositions

1.4.2 Fick's Laws

We now attempt to understand the diffusion process in terms of concentration gradients. Fick's first law which can be written as [13]

$$\vec{J} = -D\vec{\nabla}c \quad (31)$$

states that the atomic flux J will always try to minimise the concentration gradient of composition c . The proportionality constant is given the name diffusivity and the negative sign indicates the minimisation of the flux. Using the law of conservation of mass, we can write

$$\frac{\partial c}{\partial t} = -\vec{\nabla} \cdot \vec{J} \quad (32)$$

Using equation 31 we can write

$$\frac{\partial c}{\partial t} = D \nabla^2 c \quad (33)$$

The above equation is known as Fick's second law. This is the classical time dependent diffusion equation as a function of composition profile. In equation 31 the negative sign predicts that atoms will move in such a way that the flux will get minimised. The minimisation of flux would mean that the concentration gradient that exists in a system would get homogenized as shown in figure 10a. However, this is only true for an ideal system (where $\Omega = 0$) which does not show any phase separation.

For a phase separated system shown in figure 8 the diffusivity D must become negative to explain the behaviour of the system in figure 10b, so that A rich region becomes richer in A type atoms and B rich regions become richer in B type atoms.

In any system it is unclear as to why diffusivity would suddenly change sign. The initial explanation which was proposed suggested that the phenomenon was an uphill diffusion i.e. diffusion happening against the concentration gradient.

Thus it is clear that Fick's law needs to be modified to account for this behaviour. We know from thermodynamics that these alloy systems evolve in such a way that free energy gets minimised. As we saw in section 1.4.1 free energy getting minimised is the same thing as chemical potential getting equalised. So it would be more accurate to represent the Fick's law in terms of chemical potential gradient. As shown by Porter and Easterling [13], we can modify and write Fick's law to work with chemical potentials as

$$\vec{J} = -MG''\nabla^2 c \quad (34)$$

Where M is mobility and G'' represents the curvature of the free energy vs composition curve. Using equation 32 we can write

$$\frac{\partial c}{\partial t} = \frac{M}{N_v} \nabla^2 c \quad (35)$$

where we have assumed mobility and G'' to be constant. Since chemical potential was defined per atom, the N_v is introduced which represents number of atoms per mole. Thus from equation 33 and 35 we can write diffusivity as

$$D = \frac{M}{N_v} G'' \quad (36)$$

We see that if $G'' < 0$ then $D < 0$. Thus Fick's law appears to be a special case where diffusivity is positive and we can conclude that diffusivity and mobility are connected by the double derivative of the GFE which defines the sign of diffusivity D . As a consequence

we expect the diffusivity to be negative in the spinodal region.

1.4.3 Failure of Diffusion Equation

The diffusion equation (equation 33) shows that the rate of change of composition at any point in time in such a system is given by the gradient or curvature of the composition profile. The curvature tells us whether the composition at a point will increase, decrease or remain same. This can easily be shown by choosing a sinusoidal composition profile in one dimension.

The solution to the diffusion equation (35) in 1D would have the form

$$c - c_0 = A(\beta, t)e^{i\beta x} \quad (37)$$

where $\beta = \frac{2\pi}{\lambda}$. Putting this in equation 35 we get

$$A = A(\beta, 0)e^{R(\beta)t} \quad (38)$$

Where

$$R(\beta) = -\frac{M}{N_v} G'' \beta^2 \quad (39)$$

G'' defines the sign of $R(\beta)$. In the metastable region where $G'' > 0$, $R(\beta)$ will be negative and thus the exponential term will decay thus decaying the amplitude of the sinusoidal wave. So for a sinusoidal composition profile equation 35 predicts that the system will get homogenized as given in figure 11a where as a real system shows phase separation as given in figure 11b.

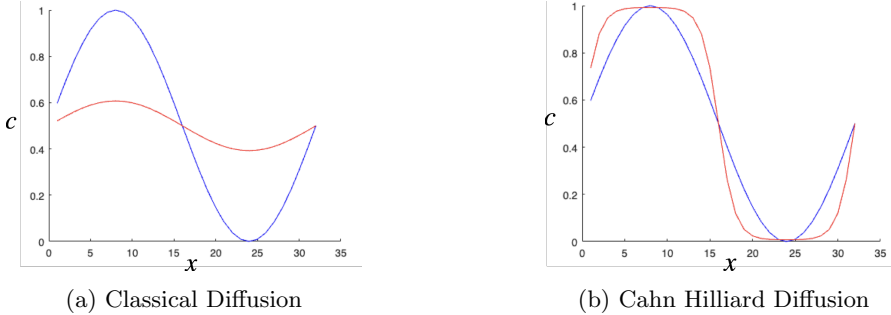


Figure 11: Evolution of 1D sinusoidal composition profile with time. Blue line corresponds to $t = 0$ and red line corresponds to $t > 0$

In the stable region where $G'' < 0$, $R(\beta)$ will be positive thus increasing the amplitude exponentially. This means that any fluctuations in the composition profile are going to grow irrespective of the wavelength. If even the smallest wavelength which is the distance between two atoms is going to grow our system will show an ordered structure at the atomic

scale. Thus, since no phase separation behaviour is predicted by our equation, we have a contradiction.

To conclude, we started with a regular solution model and assumed a system which showed spinodal decomposition i.e. $\Omega > 0$ which means our system prefers AA and BB bonds over AB bonds. We saw that there was a need for a more generalised Fick's law in terms of chemical potential since equalising chemical potential corresponds to free energy being minimised. Writing the appropriate diffusion equation gave us an understanding into how diffusivity can become negative. However negative diffusivity is not sufficient to explain phase separation since assuming negative diffusivity leads to phase separation at a very fine scale which means that the structure obtained would be ordered instead of phase separated. In essence we started with a phase separated system and solved the diffusion equation and ended up with an ordered structure instead of a phase separated one. Which means that the classical diffusion equation fails to explain phase separation even if we assume diffusivity to be negative.

1.5 Cahn-Hilliard Equation

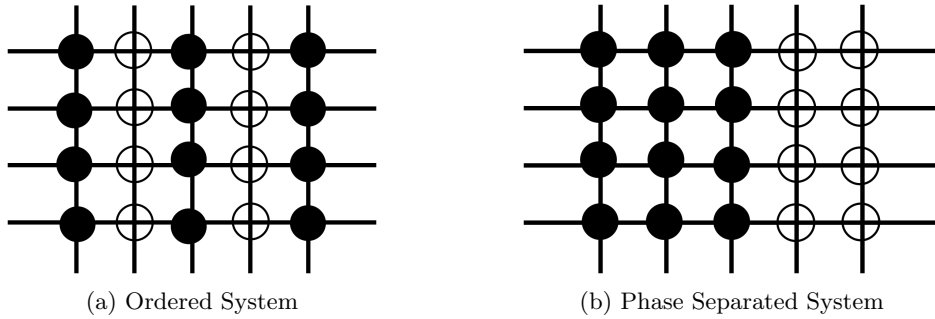


Figure 12: System configurations based on solution models

The classical diffusion equation predicts an ordered system (figure 12a) instead of a phase separated system (figure 12b). Using a discrete lattice model, Hillert figured out that the diffusion equation is missing out on the interfacial energy [8]. An interface can be defined as a region where A rich region meets B rich region. For $\Omega > 0$, AB bonds are costlier than AA and BB bonds which is why our system tries to phase separate to form the least number of AB bonds (figure 12b) but in an ordered system there are lots of AB bonds so the energy associated with the formation of interfaces is not being accounted for and thus our system is creating lots of interfaces. A lower limit to how fine this phase separation can be has been seen experimentally [6] to be of 100\AA .

Cahn in 1961[4], derived a continuum model based on Hillert's discrete lattice model and modified the diffusion equation to account for interfacial energy.

Instead of having GFE as a function of composition like we did in equation 13, Cahn and Hilliard assumed GFE to be a functional dependent of the composition as well as the derivatives of composition to account for interfaces in the system.

$$\mathbf{G} = \int F(x, y, z, c, \vec{\nabla}c, \vec{\nabla}^2c) dV \quad (40)$$

Here \mathbf{G} which is now a functional, is still a scalar quantity while $\vec{\nabla}c = \frac{\partial c}{\partial x_i}$ is a vector or a first rank tensor and $\vec{\nabla}^2c = \frac{\partial^2 c}{\partial x_i \partial x_j}$ is a second rank tensor. We can Taylor expand this functional about a function $f(c)$

$$F(c, \vec{\nabla}c, \vec{\nabla}^2c) = f(c) + \frac{\partial f}{\partial \vec{\nabla}c} \cdot \vec{\nabla}c + \frac{\partial f}{\partial \vec{\nabla}^2c} \bigotimes \vec{\nabla}^2c + \frac{1}{2!} \frac{\partial^2 f}{\partial \vec{\nabla}c \partial \vec{\nabla}c} \bigotimes \vec{\nabla}^2c \quad (41)$$

Using the Einstein summation convention we can write

$$\frac{\partial f}{\partial \vec{\nabla}c} = \frac{\partial f}{\partial \left(\frac{\partial c}{\partial x_i} \right)} = \alpha_i \quad (42)$$

$$\frac{\partial f}{\partial^2 \vec{\nabla}c} = \frac{\partial f}{\partial \left(\frac{\partial^2 c}{\partial x_i \partial x_j} \right)} = \beta_{ij} \quad (43)$$

$$\frac{\partial^2 f}{\partial \vec{\nabla}c \partial \vec{\nabla}c} = \frac{\partial^2 f}{\partial \left(\frac{\partial^2 c}{\partial x_i \partial x_j} \right) \partial \left(\frac{\partial^2 c}{\partial x_i \partial x_j} \right)} = \gamma_{ij} \quad (44)$$

where $i, j = x, y, z$

We assume a cubic crystal with isotropic and inversion symmetry. As a consequence of inversion symmetry all odd rank tensors should be 0. All second rank tensors become isotropic. Thus we can now write

$$F = f(c) + \alpha_i (\vec{\nabla}c)_i + \beta_{ij} (\vec{\nabla}^2c)_{ij} + \frac{\gamma_{ij}}{2} (\vec{\nabla}c)_i (\vec{\nabla}c)_j + \dots \quad (45)$$

We can make the β_{ij} and γ_{ij} to the same form by writing

$$\begin{aligned} \int \beta_{ij} (\vec{\nabla}^2c)_{ij} dV &= \int \beta_{ij} \left(\frac{\partial^2 c}{\partial x_i \partial x_j} \right) dV \\ &= \int \beta_{ij} \frac{\partial}{\partial x_i} \frac{\partial c}{\partial x_j} dV \\ &= \int \beta_{ij} \frac{\partial}{\partial x_i} \cdot (\vec{\nabla}c)_j dV \\ &= \beta_{ij} (\vec{\nabla}c)_j |_S - \int \frac{\partial \beta_{ij}}{\partial x_i} \cdot (\vec{\nabla}c)_j dV \end{aligned}$$

Suppose we choose the surface in such a way that the opposite surfaces will give equal contribution, then the $\beta_{ij}(\vec{\nabla}c)$ evaluated at the surface will have no contribution. Thus,

$$\int \beta_{ij}(\vec{\nabla}^2 c)_{ij} dV = - \int \frac{\partial \beta_{ij}}{\partial c} \cdot \frac{\partial c}{\partial x_i} \cdot (\vec{\nabla} c)_j dV \quad (46)$$

Hence we can write the free energy functional as

$$\mathbf{G} = \int \left\{ f(c) + \left[\frac{\gamma_{ij}}{2} - \frac{\partial \beta_{ij}}{\partial c} \right] (\vec{\nabla} c)_i (\vec{\nabla} c)_j \right\} dV \quad (47)$$

The quantity within the square brackets can be written as

$$\kappa_{ij} = \left[\frac{\gamma_{ij}}{2} - \frac{\partial \beta_{ij}}{\partial c} \right] \quad (48)$$

Where κ is the gradient energy coefficient. In a cubic system second rank tensors are isotropic so we can write $\kappa_{ij} = \kappa_{ji}$. Thus the free energy functional now becomes

$$\mathbf{G} = \int \left\{ f(c) + \kappa \delta_{ij} (\vec{\nabla} c)_i (\vec{\nabla} c)_j \right\} dV \quad (49)$$

The final form of GFE functional is written as

$$\mathbf{G} = \int \left[f(c) + \kappa (\vec{\nabla} c)^2 \right] dV \quad (50)$$

Similar to equation 26 we can write the chemical potential by taking the variational derivative of the functional \mathbf{G}

$$\mu = \frac{1}{N_v} \frac{\delta \mathbf{G}}{\delta c} \quad (51)$$

Assuming κ to be constant the variational derivative term can be evaluated as

$$\frac{\delta \mathbf{G}}{\delta c} = \frac{\partial f}{\partial c} - 2\kappa \vec{\nabla}^2 c \quad (52)$$

Similar to the derivation of equation 35 using equation 32 we can write

$$\frac{\partial c}{\partial t} = M \vec{\nabla}^2 \mu \quad (53)$$

Multiplying the above equation N_v and substituting the value calculated for chemical potential we get

$$\frac{\partial c}{\partial t} = M \vec{\nabla}^2 \left(\frac{\partial f}{\partial c} \right) - 2\kappa M \vec{\nabla}^4 c \quad (54)$$

This modified diffusion equation is known as the Cahn-Hilliard equation. We can also write

this equation as

$$\frac{\partial c}{\partial t} = M f'' \vec{\nabla}^2 c - 2\kappa M \vec{\nabla}^4 c \quad (55)$$

Here diffusivity $D = Mf''$. Thus the diffusivity depends on the mobility and the second derivative of the free energy with respect to composition. The first term in equation 55 is the classical diffusion equation and the second term incorporates a high order modification to the diffusion equation. The second term is responsible for incorporating the interfacial free energy of the system into the diffusion equation.

2 Methodology

The aim of this study is to investigate the 2 dimensional solutions of the Cahn-Hilliard equation computationally. To model the alloy system on a computer we begin by thinking of the phase field as discrete points which can be represented as a scalar field as values in a matrix. The order of this matrix can be chosen based on the size of the system we are trying to simulate. This matrix is given an initial value based on the initial composition of A-type and B-type atoms of the system. The composition profile values lie between 0 and 1 where 0 represents an A rich and 1 represents B rich regions. Hence all elements of the matrix are given the same value between 0 and 1. A random noise of the order 10^{-2} is added to the entire composition profile for getting the simulation started. Boundary conditions need to be set up next. The equations have to be non-dimensionalized before being subject to various numerical methods. First step towards solving a time dependent differential equation is to calculate all the space derivatives at a discrete point and then take a step forward in time. Different methods are used to calculate the space and time derivatives at every point. Our goal is to look for the most efficient and least computationally expensive combination of methods to study the dynamics of the phase field. Two methods are used to solve the space derivatives namely, finite difference method and spectral method. They have been described in detail in the following sections. To move the system forward in time we can use the Euler Forward, Euler Backward or Crank-Nicolson method. For this study we have only used the Euler Forward method also known as Euler explicit. This process is repeated and the simulation is run for multiple time steps. As the system moves forward in time the values of the concentration matrix changed based on CH equation. For comparing the solution of different numerical methods, the same composition profile is simulated in every program and each simulation is run for a total of 120 time units. Our system is isothermal. All programs have been written in MATLAB and are provided in the Appendix.

2.1 Simulation Parameters

Since we are going to be using spectral techniques which make use of the Fast Fourier Transform (Fast Fourier Transform (FFT)) algorithm it would be efficient to choose our matrix of the order 2^n . Thus, we begin with setting up a square matrix of order 128x128. We simulate the system for various initial compositions going from 0.1, 0.2,..., 0.9 . The values of diffusivity are kept at 1.0, and the step size for the system

$$dx = dy = 1.0 \quad (56)$$

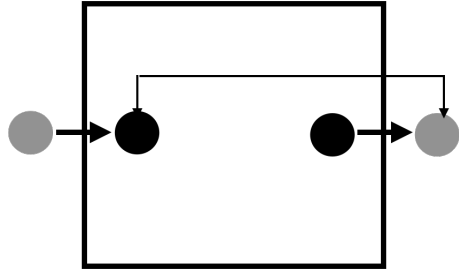


Figure 13: Periodic Boundary Condition

The size of the time-step depends on the numerical method being used. The CHequation

$$\frac{\partial c}{\partial t} = D [\nabla^2 g - 2\kappa \nabla^4 c] \quad (57)$$

where

$$g = \frac{\partial f}{\partial c} \quad (58)$$

Here f is the free energy function given in equation 13. This function however, is tough to compute computationally. Thus we choose a function similar to it which would produce the same free energy vs composition curve

$$f = Ac(1 - c)(1 - 2c) \quad (59)$$

The value of A has been kept constant at 1.0 for all simulations. Since this equation has no temperature dependence we have made an assumption that our system is isothermal. This function is used in place of the free energy function (equation 13) because the logarithmic terms in equation 13 are computationally expensive. Using equation 13 instead of this approximation would allow us to modulate the temperature as well however that is beyond the scope of this thesis. Equation 59 is a good approximation for equation 13.

2.1.1 Boundary Conditions

Several boundary conditions can be used to investigate the system. In order to simulate an infinite system, we try and model a Representative Volume Element(Representation Volume Element (RVE)) by using the Periodic Boundary Condition (Periodic Boundary Conditions (PBC)). As showing in figure 13 the PBC method assumes that the $(n + 1)^{th}$ element becomes the first element of the row and the 0^{th} element becomes the n^{th} element of the row. The same condition is also applied to all rows and columns of the matrix.

2.2 Numerical Methods

The main purpose of this study is to find the best combination of numerical methods that can be used together to solve the Cahn-Hilliard equation in the most stable and efficient way. Different numerical techniques are used to solve the space and the time derivatives. The space derivatives are solved first and then we move a step forward in time.

Cahn-Hilliard equation involves two space derivatives of order 2 and 4. These are can be calculated by either using the finite difference or the spectral method.

2.2.1 Euler Explicit Method

To compute the evolution of any system in time we need an integration method to work with our differentiation method. The time part of our equation can be written as

$$\frac{\partial c}{\partial t} = f(x, y, t) \quad (60)$$

We approximate this time derivative by taking the forward difference of the next state and the current state of the system divided by the time step. This can be written as

$$\frac{y^{t+\Delta t} - y^t}{\Delta t} = f(x_n, y_n, t_n) \quad (61)$$

Here we are using the subscript n to denote descretized values of space and time and the superscript t or $t + \Delta t$ represent the time state of the system. We can solve the above equation for the expression of the next state of the system

$$y^{t+\Delta t} = y^t + \Delta t f(x_n, y_n, t_n) \quad (62)$$

This method is intuitive and easy to implement computationally but it is explicit and of first order so the time steps must not be too large for the method to be stable.

2.2.2 Finite Difference Method

In the finite difference method we use the grid of the matrix to calculate the derivatives. It is common to use the central difference formula to calculate derivatives. Since we are solving in 2D, index i represents the x axis and j represents the y axis.

$$\nabla^2 g = \frac{g_{i+1,j}^t - 2g_{i,j}^t + g_{i-1,j}^t}{(\Delta x)^2} + \frac{g_{i,j+1}^t - 2g_{i,j}^t + g_{i,j-1}^t}{(\Delta y)^2} \quad (63)$$

$$= \frac{T_1}{(\Delta x)^2} + \frac{T_2}{(\Delta y)^2} \quad (64)$$

Here $\Delta x = \Delta y = \Delta h$ The fourth order derivative term can be written as

$$\begin{aligned}\nabla^4 c &= \frac{c_{i-2,j}^t - 4c_{i-1,j}^t + 6c_{i,j}^t - 4c_{i+1,j}^t + c_{i+2,j}^t}{(\Delta x)^4} \\ &\quad + \frac{c_{i,j-2}^t - 4c_{i,j-1}^t + 6c_{i,j}^t - 4c_{i+1,j}^t + c_{i+2,j}^t}{(\Delta y)^4}\end{aligned}\quad (65)$$

$$\nabla^4 c = \frac{T_3}{(\Delta x)^4} + \frac{T_4}{(\Delta y)^4}\quad (66)$$

We can write the time derivative part using the Euler explicit method as

$$\frac{\partial c}{\partial t} = \frac{c_{i,j}^{t+1} - c_{i,j}^t}{\Delta t}\quad (67)$$

Thus, using equation 57, we can now write the discrete form of CH equation as

$$c_{i,j}^{t+1} = c_{i,j}^t + \beta_1 T_1 + \beta_2 T_2 - \beta_3 T_3 - \beta_4 T_4\quad (68)$$

where

$$\beta_1 = \frac{D\Delta t}{(\Delta x)^2} \quad \beta_2 = \frac{D\Delta t}{(\Delta y)^2} \quad \beta_3 = \frac{2\kappa\beta_1}{(\Delta x)^2} \quad \beta_4 = \frac{2\kappa\beta_2}{(\Delta y)^2}\quad (69)$$

To solve this equation computationally we can calculate the constants β_i before hand and move our system forward in time one by one calculating the space derivatives each time.

2.2.3 Spectral Method

Spectral method uses a special property of the Fourier transform technique to calculate the derivatives. [2].

$$FT \left[\frac{\partial^n f}{\partial x^n} \right] = (ik)^n f\quad (70)$$

Using this we can easily calculate the partial derivatives present in CH equation. So the first step in the spectral method is to take our composition from real space to Fourier space.

$$c(x, y, t) \xrightarrow{\mathcal{F}} \tilde{c}(k_x, k_y, t)\quad (71)$$

Since our composition values are already discrete, we can transform them to Fourier space using the Discrete Fourier Transform method. The computationally fast and efficient way to do this is to use the Fast Fourier Transform tools present in MATLAB. Functions `fft2(c)` and `ifft2(c)` are used to transform the 2 dimensional composition matrix to Fourier Space and back to real space. So we write the CH equation as

$$\frac{\partial \tilde{c}}{\partial t} = \tilde{D} [\nabla^2 \tilde{g} - 2\kappa \nabla^4 \tilde{c}]\quad (72)$$

where all the tilda over each term is it's fourier space representation. The space derivatives as

$$\nabla^2 \tilde{g} = -(k_x^2 + k_y^2) \tilde{g} \quad \nabla^4 \tilde{c} = (k_x^4 + k_y^4) \tilde{c} \quad (73)$$

Now we can begin solving the CH equation. Since $g(c)$ is a function of composition in real space given by equation 58 and is a non-linear term we must treat it explicitly while treating all other terms implicitly. This equation can now be discretized and solved using the Euler Explicit method. Using the derivatives calculated in equation 73

$$\frac{\tilde{c}^{t+\Delta t} - \tilde{c}^t}{\Delta t} = \tilde{D}[-(k_x^2 + k_y^2)\tilde{g}^t - 2\kappa(k_x^4 + k_y^4)\tilde{c}^{t+\Delta t}] \quad (74)$$

Solving the above equation for $\tilde{c}^{t+\Delta t}$ we get

$$\tilde{c}^{t+\Delta t} = \frac{\tilde{c}^t - \tilde{D}(k_x^2 + k_y^2)\Delta t \tilde{g}^t}{1 + 2\kappa(k_x^4 + k_y^4)\Delta t} \quad (75)$$

Since we treat some part of the equation explicitly and other parts implicitly while solving, this technique is known as semi-implicit spectral technique. The Fourier space is already periodic in nature, the region we are studying is $[-\frac{\pi}{a}, \frac{\pi}{a}]$ so the value of k_x and k_y need to change accordingly. Equation 75 can be programmed easily with periodic boundary conditions in Fourier space and the system can be simulated for a number of time steps.

3 Results and Analysis

Based on the numerical solutions of the Cahn Hilliard equation the programs for simulating the 2D alloy have been written in MATLAB and have been given in appendix A and appendix B. These programs simulate the system with periodic boundary conditions thus simulating an RVE of an infinite system. The finite difference approach and the spectral approach both require careful fine tuning of the constant parameters. If not tuned properly, the system diverges giving us an incorrect simulation where phase separation is not observed. Thus programs for both methods were first optimised for time-step dt and total time-steps. A random matrix generator program was written which generated 128x128 matrices of varying initial compositions. The same matrices were used to study all simulations so we can study and compare various simulations starting under different parameters

From literature it can be shown that droplet like microstructures are observed at an initial composition of 0.3 [12]. We use this as a reference point to fine tune our parameters.

3.1 Finite Difference Approach

The finite difference approach uses the finite difference approximation to calculate derivatives. A function was written to solve for $\nabla^2 f$ in general and called twice to solve the CH equation.

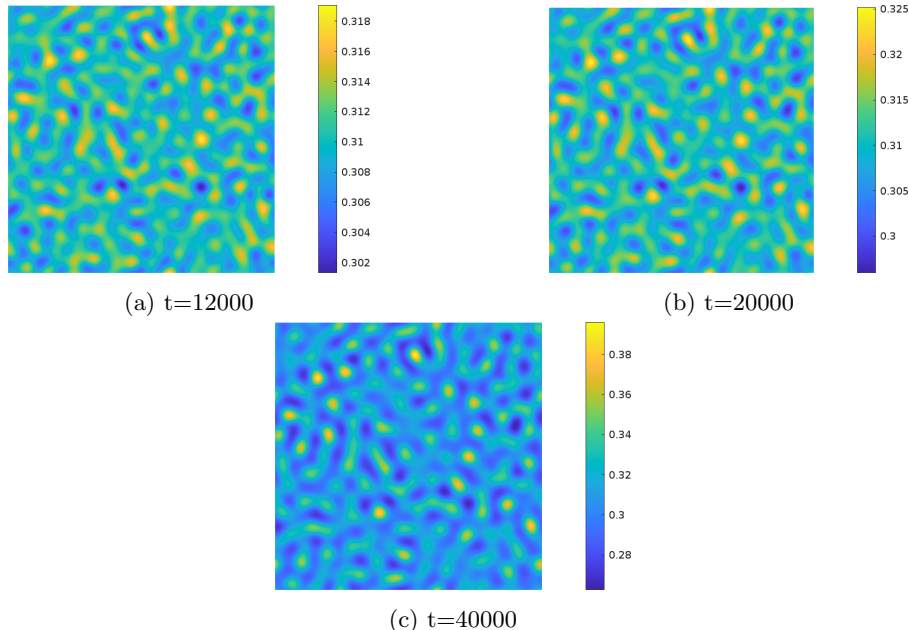
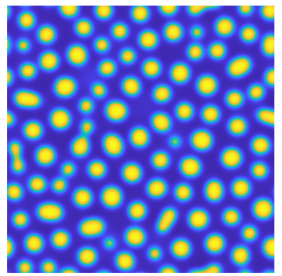
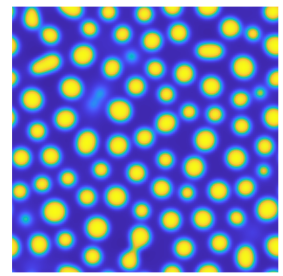


Figure 14: Total time step optimisation for $dt = 0.001$ $\kappa = 0.5$ $c = 0.3$ using the finite difference method.



(a) $t=12000$



(b) $t=20000$

Figure 15: Total time step optimisation for $dt = 0.01$ $\kappa = 0.5$ $c = 0.3$ using the finite difference method.

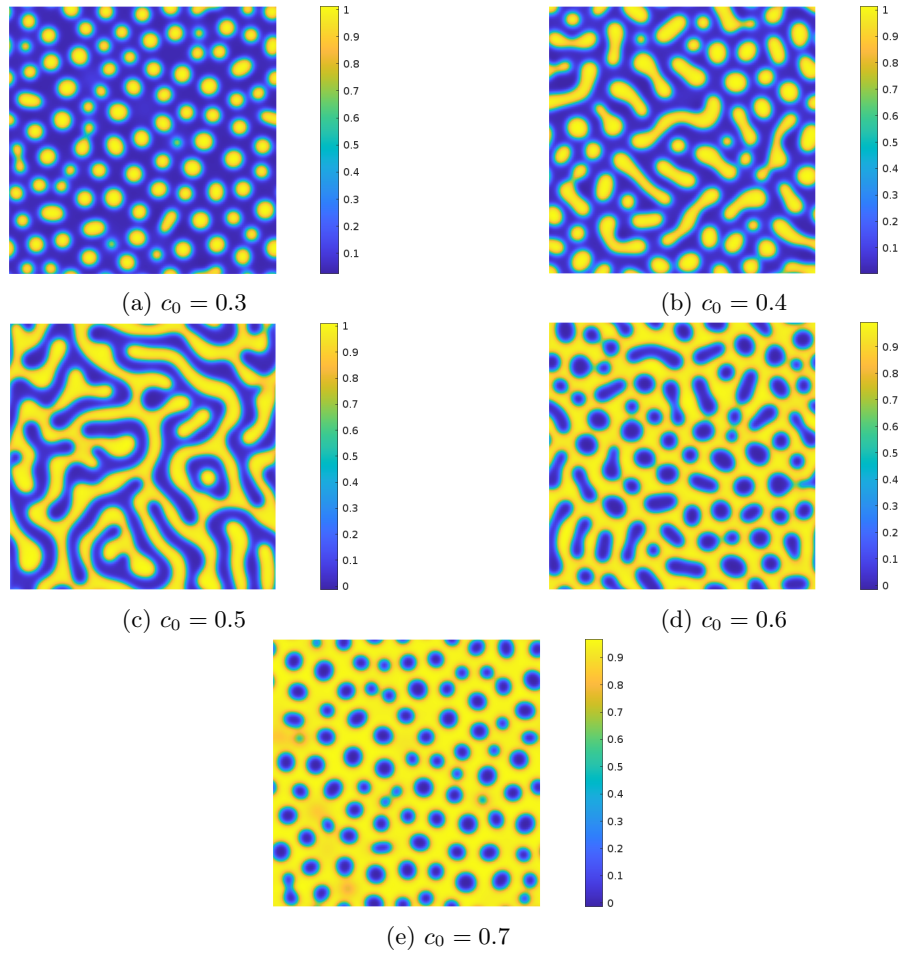


Figure 16: Phase separated systems with varying initial composition simulated using finite difference method for $dt = 0.01$ $\kappa = 0.5$ *total-time-steps* = 12000

Since value of timesteps is usually very small for finite difference approximations we start with a small dt value. In figure 14, we have simulated the system for different total time steps to see if the system converges and shows phase separation. None of the simulations displayed clear phase separation so we move to a higher value of dt .

We see that in figure 15 there isn't much difference between the simulation runs $t=12000$ and $t=20000$ and the system converges for both conditions. For $dt = 0.1$ which is a relatively large time-step the system does not converge and we obtain Not a Number (NaN) values. Thus we have found optimal values for our parameters which are $dt = 0.01$, $\kappa = 0.5$ and we run the simulation for a total of 12000 time-steps. Until now we were simulating the system for an initial composition of 0.3 which means 30% A type atoms and 70% B type atoms exist in our system. Using these parameters we simulate the system for varying initial compositions of A and B atoms. This has been shown in figure 16.

3.2 Spectral Method

Spectral method as compared to finite difference method is much more efficient since calculation of derivatives is much easier in Fourier space than it is in real space. As a consequence spectral simulations can converge in significantly less time-steps. We start by fixing the initial composition c_0 at 0.3 and run the program for various time-steps $dt = 0.5, 1.0, 1.5$. As shown in figure 17c the simulation is best at a time-step $dt = 1.5$. This is a significantly larger time-step. While running the simulations it was also found that 80 time steps is too short for some of the simulations to fully converge like the one given in figure 18 so we switch to a total of 120 time-steps.

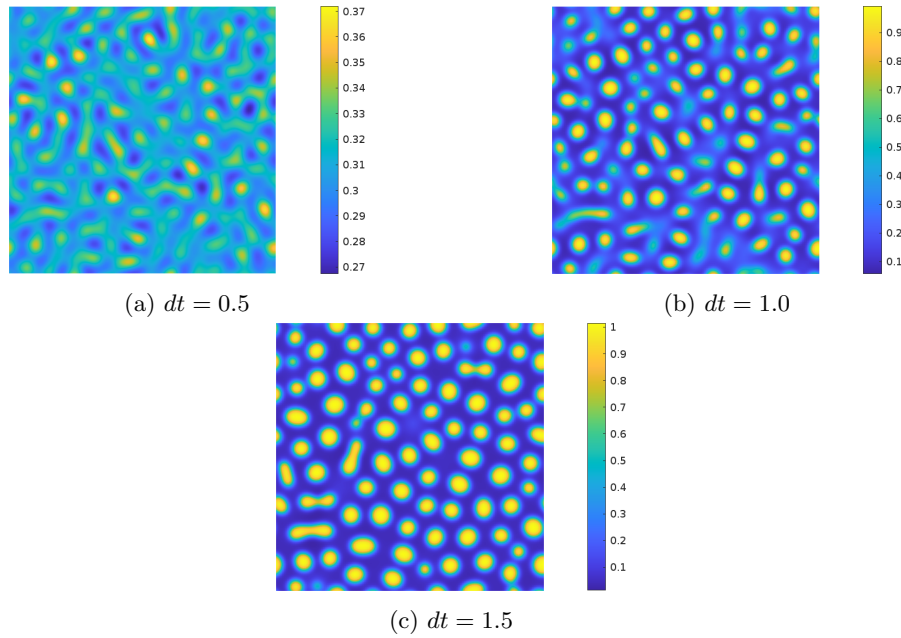


Figure 17: Time-step(dt) optimisation with $\kappa = 0.5$ $total-time-steps = 80$ for spectral method solution

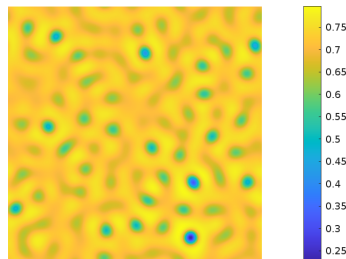


Figure 18: Spectral Method simulationn of $c_0 = 0.7$ which did not converge for $dt = 1.0$ $\kappa = 0.5$ $total-time-steps = 80$

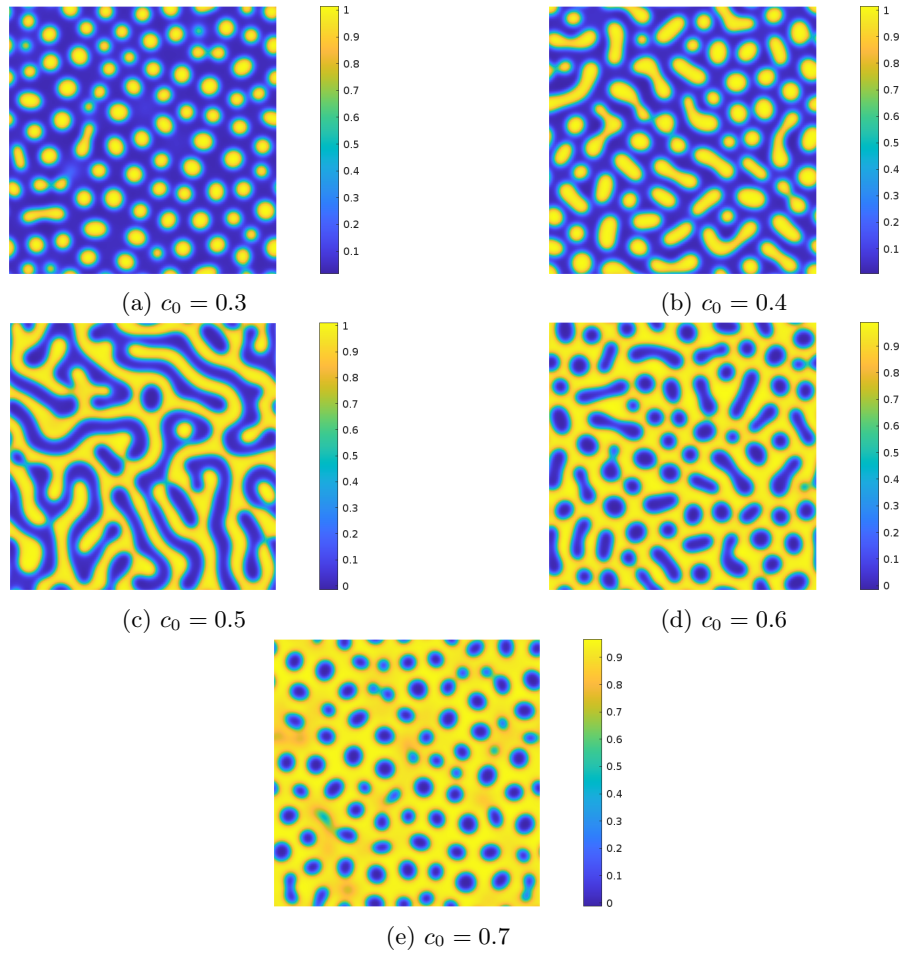


Figure 19: Phase separated systems with varying initial composition simulated using spectral method for $dt = 1.0$ $\kappa = 0.5$ total - time - steps = 120

With the parameters optimised we run the system for varying initial composition profiles. Figure 19 shows the phase separation observed as a consequence of changing the composition profile.

4 Conclusion and Future Scope of Work

- From our simulations we can conclude that the spectral method yields results much faster and is more stable than finite difference method. The simulations under finite difference method takes much longer to run as the time step (dt) value is very small and total time-steps is very large. The advantage of using Fourier transform to calculate the spatial derivatives is significant.
- We also observe droplet like microstructures and spinodal decomposition for the 0.3 initial composition. The programs developed for solving CH equations can be used to investigate microstructures of specific alloy systems and the simulation can be compared to the X-ray diffraction patterns of various alloys with different initial concentrations. This information can help in development of metallic glasses with varying microstructures.
- Many other numerical methods can also be used in combination with the numerical techniques used in this work to improve the performance, accuracy and stability of the system. Methods like backward difference or Crank-Nicolson can be used to solve the time dependence. The Adams–Bashforth method can be used to treat the implicit term of the equation.
- The function(equation 59) used in this work for approximating the free energy function given in equation 13 is a very crude approximation as it removes the temperature dependence and assumes an isothermal model. This is done to reduce computational costs as mentioned in section 2.1. However this approximation can be avoided and replaced by either equation 13 or any other thermodynamic model like the Flory Higgins thermodynamic model of polymers[11].
- The Cahn-Hilliard type diffusion applies to all systems where there is an interface present between separated phases and there is some energy associated to these interfaces. Polymers is also a good example of a system where this phenomenon is observed. The CH equation coupled with the Navier-Stokes equation of fluid flow is used to simulate the phase separation dynamics of various polymers[11].

Appendix A - Finite Difference method

This code was written in MATLAB to solve the Cahn Hilliard equation in 2D using the finite difference method. A function was developed to solve the laplacian ∇^2 on the scalar field c with periodic boundary conditions .

```
function f=lap(c)
dx=1.0;
N=size(c,1);
for i=1:size(c,1)
    for j=1:size(c,2)
        % PBC
        L=i-1;
        R=i+1;
        U=j-1;
        D=j+1;
        if(L==0) L=N;
        end
        if(R==N+1) R=R-N;
        end
        if(U==0) U=N;
        end
        if(D==N+1) D=D-N;
        end
        f(i,j)=(c(L,j)+c(R,j)+c(i,U)+c(i,D)-4*c(i,j))/((dx)^2);
    end
end
```

The main program calls this function twice to solve the Cahn-Hilliard and the algorithm has been coded in an intuitive way.

```
%Main Program
clear;
clc;
clf;

N=128;
M=128;
```

```

dx=1.0;
dy=1.0;
dt=0.001;

kappa=0.5
Mob=1.0

c_0=0.3
c=c_0+0.02*rand(N,M);
%l=load('c_0.8.mat');
%c=l.c;

for t=1:20000
    disp(t)
    g=2.*c.*(1.-2.*c).*(1.-c);
    d=lap(c);
    cnew=c+dt*Mob*lap(g-(kappa*2).*d); %algorithm
    c=cnew;
end

figure(1)
pcolor(c), shading interp, ...
axis('off'), axis('equal');
colorbar;

```

Running the main program generates a matrix with an initial composition profile of 0.3 with an error of order 10^{-2} . Then the system is propagated in time using the algorithm.

Appendix B - Spectral Method

This code was written in MATLAB to solve the Cahn Hilliard equation in 2D using the spectral method.

```
clear;
clc;
clf;
N=128;
M=N;
dx=1.0;
D=1.0;
k=0.5;
%noise=0.1*rand(N,M);
%c_0=0.4;
%c=c_0+noise;
l=load('c_0.3.mat')
c=l.c
halfN=N/2;
halfM=M/2;
dkx=2*pi/N;
dky=2*pi/M;
dt=2.0;

for timestep=1:80
    disp(timestep)
    g=2.*c.*(1.-c).*(1.-2.*c);
    c_hat=fft2(c);
    g_hat=fft2(g);
    for i=1:N
        for j=1:M
            if((i-1)<=halfN) kx=(i-1)*dkx;
            end
            if((i-1)>halfN) kx=(i-1-N)*dkx;
            end
            if((j-1)<=halfM) ky=(j-1)*dky;
            end
            if((j-1)>halfM) ky=(j-1-N)*dky;
            end
        end
    end
```

```

k2=kx*kx+ky*ky;
k4=k2*k2;
c_hat(i,j)=(c_hat(i,j)-D*dt*k2*g_hat(i,j))/(1+2*k*k4*dt);
%c_hat(i,j)=c_hat(i,j)/(1+2*k*k4*dt);
end
end
c=real(ifft2(c_hat));
end
figure(1)
pcolor(c), shading interp, ...
axis('off'), axis('equal');
colorbar;

```

References

- [1] MF Ashby and A Lindsay Greer. Metallic glasses as structural materials. *Scripta Materialia*, 54(3):321–326, 2006.
- [2] Mary L Boas. *Mathematical methods in the physical sciences*. John Wiley & Sons, 2006.
- [3] AJ Bradley. X-ray evidence of intermediate stages during precipitation from solid solution. *Proceedings of the Physical Society*, 52(1):80, 1940.
- [4] John W Cahn. On spinodal decomposition. *Acta metallurgica*, 9(9):795–801, 1961.
- [5] Jitang Fan. High-rate squeezing process of bulk metallic glasses. *Scientific Reports*, 7(1):1–8, 2017.
- [6] American Society for Metals. *Phase Transformations: Papers Presented at a Seminar of the American Society for Metals, Oct. 12 and 13, 1968*. American Society for Metals, 1970.
- [7] D.R. Gaskell. *Introduction to the Thermodynamics of Materials, Fifth Edition*. Introduction to the Thermodynamics of Materials. Taylor & Francis, 2003.
- [8] M Hillert. A solid-solution model for inhomogeneous systems. *Acta metallurgica*, 9(6):525–535, 1961.
- [9] Charles Kittel, Paul McEuen, and Paul McEuen. *Introduction to solid state physics*, volume 8. Wiley New York, 1996.
- [10] D Lamrous, MY Debili, and E Boehm-Courjault. Microstructure and phase composition of al–zn alloys. *Journal of Advanced Microscopy Research*, 8(4):266–269, 2013.
- [11] YC Li, RP Shi, CP Wang, XJ Liu, and Y Wang. Phase-field simulation of thermally induced spinodal decomposition in polymer blends. *Modelling and Simulation in Materials Science and Engineering*, 20(7):075002, 2012.
- [12] RK Mandal, RS Tiwari, Devinder Singh, and Dharmendra Singh. Influence of ga substitution on the nature of glasses in zr69. 5al7. 5-xgaxcu12ni11 and ce75al25-xgax metallic glass compositions. *MRS Online Proceedings Library*, 1757(1):13–19, 2014.
- [13] David A Porter and Kenneth E Easterling. *Phase transformations in metals and alloys (revised reprint)*. CRC press, 2009.
- [14] IM Robertson and CM Wayman. Ni5al3 and the nickel-aluminum binary phase diagram. *Metallography*, 17(1):43–55, 1984.